Unidirectional photonic circuit with a phase-change Fano resonator

Roney Thomas, Eleana Makri, and Tsampikos Kottos
Department of Physics, Wesleyan University, Middletown, Connecticut 06459, USA

Boris Shapiro
Technion-Israel Institute of Technology, Technion City, Haifa 32000, Israel

Ilya Vitebskiy
Air Force Research Laboratory, Sensors Directorate, Wright Patterson AFB, Ohio 45433, USA

We demonstrate that the integration of a phase-change material (PCM) in one of the two microresonators of a photonic circuit, coupled to a bus waveguide, can lead to unidirectional Fano resonances and to the emergence of a unidirectional transmission window. The phase change is caused by light-induced heating and is accompanied by an abrupt increase in the extinction coefficient of the PCM resonator. Due to the photonic circuit asymmetry, the critical value of the input light intensity triggering the phase change is strongly dependent on the input light direction. The latter determines the unidirectional nature of the emerging transmission window. This effect can be utilized in on-chip magnetic-free isolators and Q switches.

I. INTRODUCTION

The realization of direction-dependent wave interference phenomena has become a compelling research topic with applications in electrodynamics, acoustics, matter waves, and quantum electronics [1–6]. At the heart of this research effort is the technological demand for controllable asymmetric (e.g., unidirectional) wave transmission. On the fundamental side the challenge is to realize structures that violate the reciprocity principle in wave propagation. In the specific framework of photonics, such advances can lead to the realization of a new generation of optical isolators and circulators, unidirectional biosensors, switches, and modulators [1,2].

Traditional schemes that circumvent electromagnetic reciprocity via magneto-optical effects [7], typically require strong bias magnetic field and/or a long optical path. Although on-chip integration of such schemes is a challenging task, recent efforts along these lines have been proven successful [8,9]. Another possible solution is to use an active approach based on spatiotemporal modulation of the material parameters, such as the refractive index. The latter can be provided by electric, acoustic, mechanical, or optical dynamic biasing [10–17]. At optical frequencies, though, it is hard to achieve spatiotemporal modulation of the refractive index, which would be strong enough for practical purposes. In addition, due to strong temporal modulation, the input and output signals might have different frequency composition for either direction of propagation. Alternative schemes involve spatially asymmetric nonlinear photonic structures [18–23]. The nonlinear effects in transmission can be different for the forward and backward propagating wave, thus resulting in intensity-dependent propagation asymmetry. One problem with this approach is associated with the relative weakness of nonlinear optical interactions, such as the Kerr effect.

In this paper, we invoke a different approach to the realization of strong asymmetry in wave propagation. Our approach does not rely on externally imposed modulation, magneto-optical nonreciprocity, or optical nonlinearity. Instead, we use the effect of self-induced heating on light transmission by a reciprocal but spatially asymmetric photonic circuit. In a free-space setting, a similar mechanism of transmission asymmetry was considered in [24,25], where a plane wave was incident on an asymmetric multilayer with a phase-change component (VO_2). The PCM loaded layered structures in [24,25] act as an asymmetric power limiter: it displays symmetric transmittance at low-input light intensity, but the transmittance becomes highly asymmetric when the input power exceeds a certain level. In this paper, we consider a qualitatively different setting, which involves a bus waveguide side coupled to an asymmetric pair of microresonators (a photonic metamolecule). The first resonator incorporates a phase-change material (PCM) which can be thermally driven to an abrupt transition from the phase with lower absorption to the state with higher absorption. In our numerical example, the PCM is vanadium dioxide (VO_2), which undergoes insulator-to-metal (ITM) phase transition just above the room temperature [26]. By contrast, the other resonator is characterized by a small but fixed extinction coefficient, which can be of the radiative nature. At low-input light intensity, the PCM of the first resonator remains in the low-temperature, dielectric phase, and the system displays a sharp Fano resonance [27,28], thereby blocking the wave propagation in either direction. The Fano resonance is a result of interaction between a high-Q resonant mode supported by the photonic metamolecule and the continuum of states supported by the

bus waveguide. The PCM resonator has some small initial absorption, which results in the light-induced heating. If the input light intensity exceeds a certain threshold, it triggers the ITM phase transition in the PCM resonator. The important point is that this threshold is strongly dependent on the direction of light propagation. Specifically, if the input light approaches the metamolecule from the side of the PCM resonator (hereinafter, the forward propagating light), the heating occurs faster, compared to the case when the light of the same intensity approaches the metamolecule from the side of the second resonator (hereinafter, the backward propagating light). The abrupt increase in absorption, associated with the proximity of the ITM transition, spoils the high Q of the resonant mode, thereby suppressing the Fano resonance and giving its place to a transmission window. For the forward propagating light, the transition occurs at lower-input light intensity than for the backward propagating light, implying the existence of a unidirectional transmission window above the ITM threshold. We find that this unidirectional Fano effect can lead to a transport asymmetry which is as high as 45 dB and has a frequency range which extends over several resonance linewidths.

The structure of the paper is as follows: In Sec. II we analyze the transport properties of the phase-change photonic circuit. Specifically, in Sec. II A we present the photonic circuit and discuss the basic optical properties of the PCM resonator. In Sec. II B we present the steady-state equations governing the transport properties of the system as well as the associated numerical scheme. In Sec. II C we present our numerical results and analyze the interference mechanisms underlying the transport properties of the circuit for various input wave intensities. Specifically, we analyze the nature of the Fano interference and the way it disappears as the result of the ITM transition in the PCM resonator. Finally, in Sec. III we present a simple theoretical model explaining the basic physics behind the unidirectional Fano resonances and the emergence of a unidirectional transmission window. Our conclusions are given in the last Sec. IV.

II. UNIDIRECTIONAL FANO RESONANCES IN PHASE-CHANGE PHOTONIC CIRCUITS

In this section we present the transport characteristics of the phase-change photonic circuit. First (Sec. II A), we describe the components of the two coupled microresonators that constitute our circuit and the optical properties of the PCM that is used. A typical optical PCM can be reversibly switched between two phases with different refractive index, optical absorption, or electrical conductance. The phase change can be caused by the input light itself (self-induced phase transitions) due to heating or some other physical mechanism [29–31]. Alternatively, it can be induced by external heating or cooling, by application of an electric or magnetic field, or by mechanical stress [32–34]. Here, we exclusively consider PCMs that undergo a self-induced phase transition due to the heating generated by the incident radiation.

In Sec. II B we present the steady-state equations that describe the transport in the presence of a PCM while a more thorough analysis of the numerical results is done in the following Sec. II C. In this section we analyze the physical
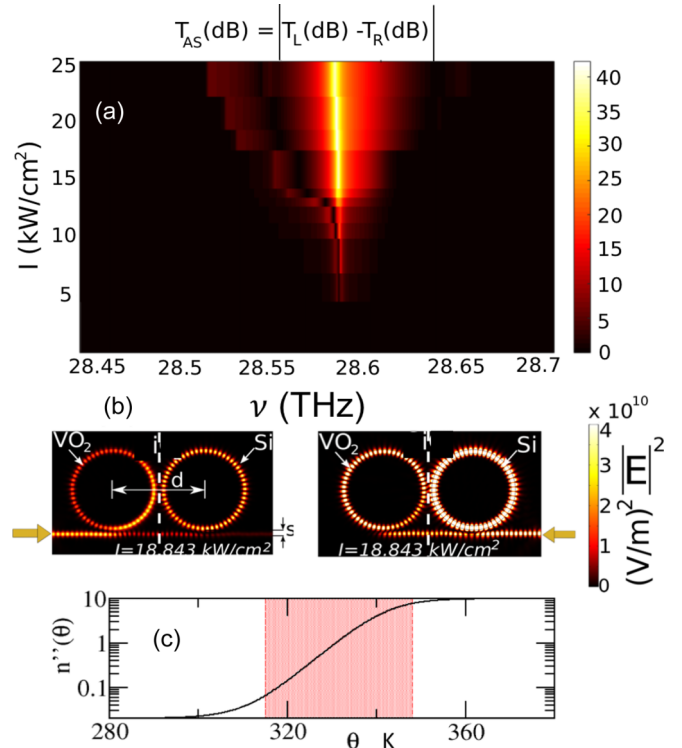
FIG. 1. (a) A density plot of left-right spectral transmittance asymmetry $T_L - T_R$ (in dBs) versus frequency ν (x axis) of the incident CW, for various values of its irradiance $\mathcal{I}$ (y axis). (b) A density plot of the scattering field intensity inside the circuit when it is illuminated with a CW signal from the left (right) direction. The frequency of the incident CW is at the Fano resonant frequency $\nu \approx 28.58$ THz and its irradiance is 18.843 kW/cm^2. (c) The dependence [Eq. (1)] of the imaginary part of the index of refraction n'' of the PCM from the temperature θ. The red highlighted area indicates the temperature regime where the Q factor of the PCM resonator is spoiled, leading to a destruction of the Fano mechanism.

mechanism that leads to the presence of unidirectional Fano resonances. As a potential application, we show that such behavior can lead to asymmetric transport with asymmetry contrasts as high as 45 dBs. The unidirectional spectrally sharp Fano effect, and the associated strong field enhancement, can be utilized for a variety of other applications (i.e., apart from asymmetric transport) such as unidirectional low-threshold lasing, enhanced nonlinear response, and (bio)sensing.

A. Photonic circuit based on phase-change materials

The proposed photonic circuit [see Fig. 1(a)] is designed to operate at the middle-infrared (MIR) regime of 10.5 μm. It consists of two ring resonators, side coupled to a straight dielectric waveguide. The bus waveguide and the right ring resonator are made of lossless Si with refractive index $n_{Si} = 3.3$. The other (left) resonator is made of a PCM which has a temperature-dependent complex refractive index $n_{PCM} = n'_{PCM}(\theta) + i n''_{PCM}(\theta)$. The thicknesses of the bus waveguide and the ring resonators are kept at 1.7 μm. The center-to-center distance d between the two ring resonators, and between the rings and the straight waveguide s, were kept fixed at $d = 35.8$ μm and $s = 2.295$ μm, respectively. The whole

circuit lays on top of a ZnS substrate with refractive index $n_{ZnS} = 2.2$.

The material used for the PCM ring is VO_2, which undergoes a phase transition from a monoclinic insulating phase to a rutile metallic phase around temperature $\theta_c = 342$ K. When the temperature drops below θ_c, the dielectric phase is restored and the material becomes optically transparent again. Furthermore, with the exception of a small hysteresis, only one of the two phases is stable at any given temperature: the dielectric phase is only stable below the phase transition temperature θ_c, while the metallic phase is stable above θ_c. The phase-change transition is reflected in an abrupt variation of the imaginary part of the index of refraction $n''_{PCM}(\theta)$ which can be as high as three orders of magnitude (depending on the deposition methods, etc.) [see Fig. 1(c)]. At the same time, the real part of the index of refraction $n'_{PCM}(\theta)$ undergoes a relatively smooth variation. We have modeled these temperature-driven variations in real and imaginary parts of the refractive index of VO_2 at the operational wavelength of 10.5 μm by a direct fit of available experimental data found in the literature [35]. The best fit is represented by the following expressions:

$$n'_{PCM}(\theta) = n'_0 + \frac{\Delta n'}{\exp[-(\theta - \theta_c)/\Delta\theta] + 1}, \quad (1a)$$

$$n''_{PCM}(\theta) = n''_0 + \frac{\Delta n''}{\exp[-(\theta - \theta_c)/\Delta\theta] + 1}, \quad (1b)$$

where $n'_0 = 3.3$ and $n''_0 = 0.001$, $\Delta\theta = 5$ K denotes the smoothing parameter over which the phase transition takes place, and $\Delta n' = 3.323$, $\Delta n'' = 8.8$ indicate the "heights" of the jumps of the optical parameters during the phase transition. Below, we will be considering the scenario for which the phase change from the dielectric to metallic state is caused by incident light-induced heating.

Finally, each of the ring resonators are designed to support a resonant mode at the mid-infrared wavelength of 10.5 μm, corresponding to their optical mode number $m = 27$. Using eigenmode analysis via COMSOL multiphysics software [36], the quality factors of the resonant optical modes supported by the lossless silicon ring and the lossy PCM ring (in the insulating phase) are evaluated as $Q_{Si} = 2.026 \times 10^4$ and $Q_{PCM} = 1.855 \times 10^3$, respectively.

B. Electromagnetic transport equations in the presence of phase-change materials

The electromagnetic wave propagation in the presence of a PMC component is a challenging computational problem [37,38]. It involves a simultaneous solution of Maxwell's equations together with a heat-transfer equation which controls the temperature variation of the optical parameters of the PCM. In the steady-state regime, the problem collapses to the following set of coupled differential equations:

$$\vec{\nabla} \times \vec{E} = i\mu_0\mu_r\omega\vec{H},$$
$$\vec{\nabla} \times \vec{H} = -i\epsilon_0 n^2(\vec{r}, \theta)\omega\vec{E}, \quad (2a)$$

$$-\vec{\nabla} \cdot (k(\vec{r})\vec{\nabla}\theta(\vec{r})) = Q(\vec{r}, \theta), \quad (2b)$$

$$Q(\vec{r}, \theta) = \epsilon_0\omega n'(\vec{r}, \theta)n''(\vec{r}, \theta)|\vec{E}|^2, \quad (2c)$$

where $\vec{E}$ and $\vec{H}$ denote the electric and magnetic field vectors, $\mu_0(\epsilon_0)$ is the permeability (permittivity) of free space, $\mu_r = 1$, and $n'(\vec{r}, \theta)$, $n''(\vec{r}, \theta)$ are position- and temperature-dependent functions that describe the real and imaginary parts of the index of refraction inside the circuit. Furthermore, the parameter $k(\vec{r})$ in Eq. (2b) describes the thermal conductivity which, at the VO_2 ring, takes the value $k_{VO_2} = 4\frac{W}{mK}$. We also assume that the ambient temperature at the edges of the surrounding ZnS substrate is constant $\theta_0 = 293.15$ K. Finally, Q [see Eq. (2c)] is the heat production (per unit volume) which is generated at the lossy VO_2 ring resonator when the energy of the incident beam is dissipated there. The generated heat, in turn, leads to an increase in the temperature of the VO_2 ring resonator, which modifies its optical parameters $n'(\theta)$ and $n''(\theta)$ as shown in Eqs. (1).

The steady-state values of transmittance T_L/T_R, phase transmission ϕ_L/ϕ_R, and temperature θ_L/θ_R, for left (L) and right (R) incident CWs (at various frequencies ν) have been evaluated by solving numerically Eqs. (2b) and (2c), using a frequency-stationary modulo of COMSOL MULTIPHYSICS [36]. In order to maintain a high accuracy of our simulation results, we have used mesh elements of sizes 0.32 and 1.312 μm within the bus and ring resonator waveguides and ZnS substrate. Throughout our simulations we have used a tolerance factor of 0.1% as a convergence criteria. The accuracy of our calculation has been further checked by doubling the mesh density. Additionally, port or reflectionless boundary conditions were used for launching and exiting electromagnetic waves within the model.

In all our simulations below, we have not considered dispersion phenomena for $n'(\vec{r})_{PCM}$, $n''(\vec{r})_{PCM}$. This approximation is justified by the fact that the variations of the index of refraction of the PCM due to temperature changes are much greater compared to any variations due to dispersion effects.

C. Unidirectional Fano interference and asymmetric transport

The outcome of the simulations has been analyzed and categorized according to the existence (or not) of sharp Fano resonance dips at the transmission spectrum. We have found two distinct behaviors associated with the value of the irradiance of the incident continuous waves (CW): (a) CW irradiances that support bidirectional (i.e., for both left and right incident waves) Fano resonance effects; (b) CW irradiances that support unidirectional Fano effects, i.e., the Fano resonance is suppressed when the incident CW enters the photonic circuit from a specific direction. As a result, the asymmetry contrast between left and right transmittances acquires high values in this regime.

An overview of the left-right transmittance asymmetry, as we increase the irradiance $\mathcal{I}$ of the incident wave, is shown in Fig. 1(a). We find that the left-right transmittance asymmetry increases, both in magnitude and in bandwidth, as $\mathcal{I}$ increases. In Fig. 1(b) we report (in a density plot) the scattering field inside the photonic circuit for a left and a right incident wave for a CW with moderate incident irradiance $\mathcal{I} = 18.843$ kW/cm². We point out that higher values of the irradiance are physically irrelevant since they correspond to electric field amplitudes of the incident wave that are above the electrical breakdown limit of the photonic circuit. In our analysis below we ignore
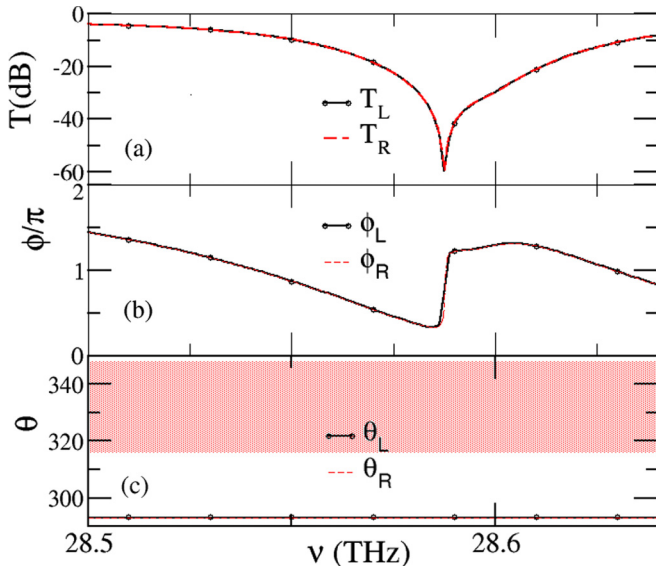
FIG. 2. (a) Transmittance $T_{L/R}$, (b) transmission phase $\phi_{L/R}$, and (c) temperature $\theta_{L/R}$ versus the frequency ν of an incident CW with irradiance $\mathcal{I} \approx 4.4$ kW/cm^2. Left (solid black lines) and right (dashed red lines) incident CW is indicated with the subindex L and R, respectively. The red highlighted area in (c) indicates the temperature domain where the variation of n''_{PCM} is approximately one order higher than its value in the dielectric phase. When the PCM temperature is in this range, the Fano resonance is typically destroyed.

this regime and focus our analysis solely to low and moderate values of irradiances of the incident wave.

In Figs. 2 and 3 we show typical results for CW with low and intermediate irradiances, respectively. Let us first consider the low irradiance case. From the numerical data shown in Fig. 2 we see that in this case all transport parameters for left and right incident waves fall one on top of the other. Specifically, from the data shown in Figs. 2(a) and 2(b) we deduce that our photonic circuit can support the formation of a sharp Fano resonance dip for both left and right incident waves at $\sim{-}60$ dB at $\nu = 28.5872$. A calculation of the steady-state temperature at the PCM resonator indicates that it remains much below θ_c for both left and right incident waves [see Fig. 2(c)]. The existence of the Fano resonance in similar types of configurations has been well documented in the literature and therefore it is not a surprise that a similar phenomenon occurs in our system as well. Its origin is traced back to the presence of fragile interference effects between two (or more) scattering paths being present in our photonic circuit: one of them involves a resonant process during which the incident wave is exciting a high-Q resonant (quasibound) state of the photonic circuit while the other scattering path involves a state within the continuum which is supported by the bus waveguide. Traces of these interference effects can be found in the transmittance T and the transmission phase ϕ when they are plotted versus the incident frequency ν [see Figs. 2(a) and 2(b)]. Specifically, in the proximity of the bound-state frequency, these quantities undergo abrupt variations, with the phase changing by π within a spectral interval proportional to the resonance linewidth. At the same
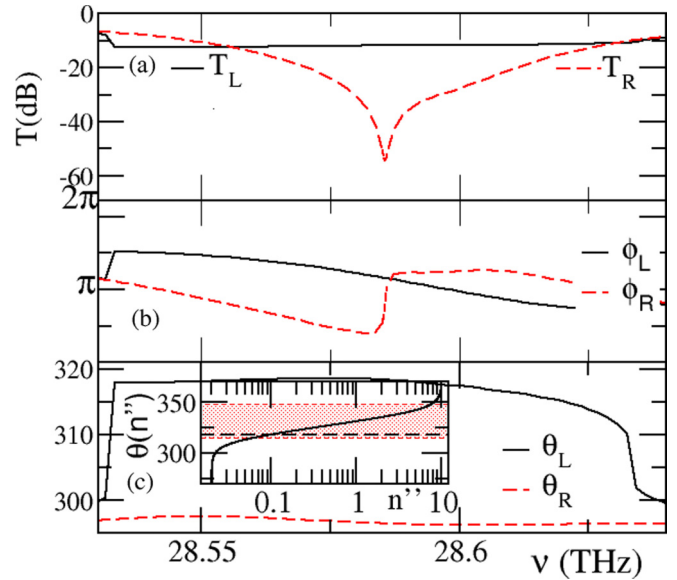
FIG. 3. (a) Left T_L (solid black lines) and right T_R (dashed red lines) transmittances for a CW entering a photonic circuit (see inset) consisting of two coupled resonators with the left resonator made by a PCM material (VO$_2$). (b) Transmission phase for a left ϕ_L and right ϕ_R incident wave versus the incident frequency ν, and (c) associated temperature θ_L (θ_R) for a left (right) incident CW wave versus the incident frequency ν. In the inset we show the variation of the imaginary part of the refractive index n'' versus the temperature θ of the PCM. The red highlighted area indicates the regime for which Fano resonances have been destroyed. The bold black dashed line indicates the value of $\theta \approx 318$ K associated with θ_L [see main panel of Fig. 3(c)]. In all cases, the irradiance of the incident CW is $\mathcal{I} \approx 18.843$ kW/cm^2.

time, the left and right transmittance profiles are equal $T_L = T_R$ and they acquire a non-Lorentzian asymmetric shape due to the destructive interference between the two paths.

The situation is completely different for intermediate values of the irradiance of the incident wave [see Figs. 3(a)–3(c). This regime is associated with irradiances which can induce temperature increase of the PCM material in a range around θ_c. In such cases, the directionality of the incident wave might affect dramatically the fragile Fano interference. Specifically, due to the asymmetric design of the photonic circuit, a left or right propagating wave might encounter different losses before engaging with the PCM resonator. As a result, they will carry different amount of energy and thus their efficiency to create a sizable increase of n''_{PCM} (or even to induce an insulator-to-metal transition) at the PCM resonator will be different.

Let us discuss in more detail the transport scenario in each of the cases associated with right and left incident CWs. Consider, for example, the situation where the CW enters the circuit from the side of the Si resonator (right incident direction). In this case, the light originally is trapped inside the Si resonator [see Fig. 1(b)] for a long time. Before it will be coupled back to the bus waveguide, a portion of its carried energy is already lost due to the radiative losses from the Si resonator. As a result, the remaining energy is not enough to raise the temperature (via absorption) of the PCM resonator,

and induce an increase of n''_{PCM} [see Fig. 3(c)]. Thus, the latter remains in the dielectric phase, and the involved Fano interference mechanisms lead to a transport behavior which is similar to the one found in the case of incident waves with low irradiances. From Fig. 3(a), we see that T_R exhibits an asymmetric resonance line shape at approximately $\nu \approx 28.58$ THz. At this frequency, the transmission phase ϕ_R undergoes an abrupt change by π, a signature of Fano interference. Finally, the temperature θ_R at the PCM resonator remains well beyond the critical temperature θ_c [see Fig. 3(c)]. As a consequence, the index of refraction (specifically n'') remains essentially constant and equal to the VO$_2$ value at the dielectric phase (see inset of this figure).

On the other hand, when the incident CW enters the photonic circuit from the side of the VO$_2$ resonator, its efficiency to heat up the PCM to temperatures that enforce sizable increases of the refraction index n''_{PCM} (say by an order from the dielectric value) remains intact. Such variations of n'' spoil the high-Q resonant mode of the photonic circuit. Consequently, the scattering path associated with the resonant mode is suppressed together with the Fano interference occurring between this path and scattering paths supported within the continuum of states from the bus waveguide. This leads to the emergence of a transparency window and an asymmetric transport between the left and right transmittance which can be as high as 45 dBs. The destruction of the Fano interference mechanism is also reflected in the transmission phase ϕ_L which varies smoothly across the resonant frequency [Fig. 3(b)]. In this frequency range, the temperature at the PCM resonator has been raised to values $\theta_L \approx 318$ K. Although this value is below the phase transition temperature θ_c, it is, nevertheless, high enough to induce a variation in $n''_{PCM}(\theta)$ of the PCM which is approximately an order of magnitude larger than the corresponding value of the insulating phase [see inset of Fig. 3(c) where $\theta_L \approx 318$ K is indicated with bold dashed black line inside the red highlighted area].

Finally, for the irradiances that we have used in this study, the time needed to destroy the Fano effect (due to a sizable increase of n''_{PCM}) is of the order of fractions of millisecond (i.e., approx. 0.1–0.5 ms). This time can be further decreased by incorporating a thermal isolation layer between the VO$_2$ and the substrate. Moreover, we point out that as far as the temperature swings are concerned, the proposed design will only work if the initial temperature is below that of the insulator-to-metal phase transition in VO$_2$, which is around $68\,^\circ$C.

III. SEMIANALYTICAL MODEL BASED ON COUPLED OSCILLATORS WITH A TEMPERATURE-DEPENDENT DAMPING COEFFICIENT

In order to obtain a quantitative understanding of the asymmetric transport hosted by the photonic circuit of Fig. 1, we analyze a simple model consisting of coupled oscillators. In particular, we model the bus waveguide as an infinite chain of identical masses m coupled by springs with constant K_0 (see Fig. 4). The ring resonators are represented by two oscillators of equal mass, each of which is coupled with one mass in the infinite array with a spring of constant K_l. The two masses are also coupled to each other with spring constant
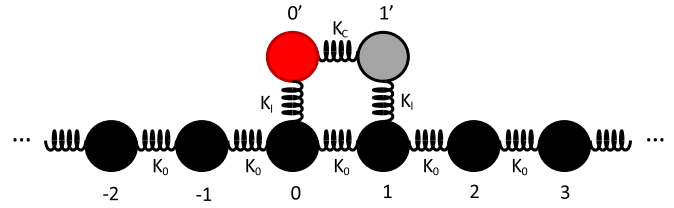
FIG. 4. Mechanical oscillator analog of the photonic circuit of Fig. 1. Two coupled oscillators, one of which has temperature-dependent friction (red), are side coupled to an infinite array (lead) of identical masses coupled with identical springs.

K_c. The resonator on the left is assumed to have losses due to friction μ. Later, we are going to incorporate a temperature dependence in analogy with the temperature-dependent optical parameters of the VO$_2$ resonator in the photonic circuit of the previous section. The system is described by the following set of equations:

$$\ddot{X}_n = -\omega_0^2(2X_n - X_{n-1} - X_{n+1}) - \omega_l^2(X_n - X_{0'})\delta_{n,0}$$
$$\qquad - \omega_l^2(X_n - X_{1'})\delta_{n,1}, \tag{3a}$$

$$\ddot{X}_{0'} = -\omega_c^2(X_{0'} - X_{1'}) - \omega_l^2(X_{0'} - X_0) - \gamma \dot{X}_{0'}, \tag{3b}$$

$$\ddot{X}_{1'} = -\omega_c^2(X_{1'} - X_{0'}) - \omega_l^2(X_{1'} - X_1), \tag{3c}$$

where $\omega_0 = \sqrt{K_0/m}$, $\omega_l = \sqrt{K_l/m}$, $\omega_c = \sqrt{K_c/m}$, and $\gamma = \mu/m$ is the damping coefficient of the oscillator on site $0'$. Above, Eq. (3a) is the equation of motion describing the nth mass in the infinite array, Eq. (3b) is the equation of motion for the lossy resonator $0'$, and Eq. (3c) is the equation of motion for the mass $1'$. The radiative losses in this model are controlled by the coupling constant k_l (though one could also introduce a small constant friction term at oscillator $n = 1'$ to imitate additional "radiative" losses).

Substituting the form $X_n(t) = a_n e^{-i\omega t}$ in the equations above we get

$$-\omega^2 a_n = -\omega_0^2(2a_n - a_{n-1} - a_{n+1}) - \omega_l^2(a_n - a_{0'})\delta_{n,0}$$
$$\qquad - \omega_l^2(a_n - a_{1'})\delta_{n,1}, \tag{4a}$$

$$-\omega^2 a_{0'} = -\omega_c^2(a_{0'} - a_{1'}) - \omega_l^2(a_{0'} - a_0) + i\gamma\omega a_{0'}, \tag{4b}$$

$$-\omega^2 a_{1'} = -\omega_c^2(a_{1'} - a_{0'}) - \omega_l^2(a_{1'} - a_1). \tag{4c}$$

From Eq. (4a) we can easily find out that a propagating wave on the infinite chain has a dispersion relation $\omega = 2\omega_0 \sin(\frac{k}{2})$. Below, we measure everything in units of $\omega_0 = 1$.

We proceed with the analysis of the transport properties of the system of Fig. 4. To this end, we consider an excitation through the infinite chain of coupled masses. For left incidence, the appropriate scattering boundary conditions are

$$a_n = I_L e^{ikn} + R_L e^{-ikn}, \quad n \leqslant 0 \tag{5a}$$

$$a_n = T_L e^{ikn}, \quad n > 0. \tag{5b}$$

Applying these boundary conditions to Eqs. (4) using $n = 0$, $n = 1$ for Eq. (4a), we obtain the following system of

equations:

$$\omega^2(I_L + R_L) = \omega_0^2[2(I_L + R_L) - I_L e^{-ik} - R_L e^{ik} - T_L e^{ik}]$$
$$+ \omega_l^2(I_L + R_L - a_{0'}), \tag{6a}$$

$$\omega^2 T_L e^{ik} = \omega_0^2(2T_L e^{ik} - I_L - R_L - T_L e^{2ik})$$
$$+ \omega_l^2(T_L e^{ik} - a_{1'}), \tag{6b}$$

$$\omega^2 a_{0'} = \omega_c^2(a_{0'} - a_{1'}) + \omega_l^2[a_{0'} - (I_L + R_L)]$$
$$- i\gamma\omega a_{0'}, \tag{6c}$$

$$\omega^2 a_{1'} = \omega_c^2(a_{1'} - a_{0'}) + \omega_l^2(a_{1'} - T_L e^{ik}), \tag{6d}$$

which allows us [using Eqs. (6a) and (6b)] to obtain the transmitted and reflected wave amplitudes in terms of the incident wave amplitude I_L, γ, and $a_{0'}$, $a_{1'}$:

$$T_L = \frac{a_{0'}\omega_l^2\omega_0^2 + a_{1'}\omega_l^2(e^{-ik}\omega_0^2 + \omega_l^2) - 2iI_L\omega_0^4\sin k}{2\omega_l^2\omega_0^2 + e^{ik}\omega_l^4 - 2i\omega_0^4\sin k}, \tag{7a}$$

$$R_L = \frac{a_{0'}\omega_l^2(\omega_0^2 + e^{ik}\omega_l^2) + a_{1'}\omega_l^2\omega_0^2 e^{ik} - I_L e^{ik}\omega_l^2(\omega_l^2 + 2\omega_0^2\cos k)}{2\omega_l^2\omega_0^2 + e^{ik}\omega_l^4 - 2i\omega_0^4\sin k}. \tag{7b}$$

The associated transmittance from the left is $\mathcal{T}_L \equiv |T_L/I_L|^2$ and can be evaluated explicitly using Eqs. (7), (6c), and (6d).

Using the same steps as above, we can calculate the transport for the case of a right incident wave. In this case, the associated boundary conditions are

$$a_n = I_R e^{-ikn} + R_R e^{ikn}, \quad n \geqslant 1 \tag{8a}$$

$$a_n = T_R e^{-ikn}, \quad n < 1 \tag{8b}$$

which leads to the following expressions for the transmission and reflection amplitudes:

$$T_R = \frac{a_{0'}\omega_l^2(\omega_0^2 + \omega_l^2 e^{ik}) + a_{1'}\omega_l^2\omega_0^2 e^{ik} - 2iI_R\omega_0^4\sin k}{2\omega_l^2\omega_0^2 + e^{ik}\omega_l^4 - 2i\omega_0^4\sin k}, \tag{9a}$$

$$R_R = \frac{a_{0'}\omega_l^2\omega_0^2 + a_{1'}\omega_l^2(\omega_0^2 e^{-ik} + \omega_l^2) - I_R e^{-ik}\omega_l^2(\omega_l^2 + 2\omega_0^2\cos k)}{2\omega_l^2\omega_0^2 + e^{ik}\omega_l^4 - 2i\omega_0^4\sin k}, \tag{9b}$$

where $a_{0'}$, $a_{1'}$ are obtained by solving the following equations:

$$\omega^2 a_{0'} = \omega_c^2(a_{0'} - a_{1'}) + \omega_l^2(a_{0'} - T_R) - i\gamma\omega a_{0'}, \tag{10a}$$

$$\omega^2 a_{1'} = \omega_c^2(a_{1'} - a_{0'}) + \omega_l^2(a_{1'} - I_R e^{-ik} - R_R e^{ik}). \tag{10b}$$

The associated transmittance from the right is $\mathcal{T}_R \equiv |T_R/I_R|^2$ and can be evaluated explicitly using Eqs. (9), (10a), and (10b).

Next, we introduce the temperature dependence of the damping coefficient γ. The underlying assumption of the calculations below is the validity of an adiabatic approximation, i.e., the heat release during one period of the oscillation is infinitesimally small. This allows us to assume that the relative change in the friction coefficient $\gamma(\theta)$ of the oscillator at site $0'$ (see Fig. 4) during one oscillation period is extremely small.

We use the following functional dependence of the friction coefficient γ from the temperature:

$$\gamma(\theta) = \gamma_{\min} + \frac{\gamma_{\max} - \gamma_{\min}}{\exp[-(\theta - \theta_c)/\Delta] + 1}, \tag{11}$$

where $\gamma_{\max}$ and $\gamma_{\min}$ are the maximum and minimum values of the damping coefficient, respectively, and Δ is a smoothing parameter. The functional form (11) is inspired by the temperature dependence of the imaginary part of the refractive index for the PCM material that was used in our optical simulations [see Eq. (1a)]. For simplicity of the analysis, we do not consider here changes of the resonant frequency of the oscillator which would correspond to the change in real refractive index with temperature in the optical setup.

The change in temperature at the mass with friction involves two terms: (a) a heating term, which is the time-averaged power dissipated due to friction that causes the heating and (b) a cooling term which describes the dissipation of heat. The heat rate equation is then

$$\frac{d\theta(t)}{dt} = -\kappa[\theta(t) - \theta_0] + \overline{P(t)}, \tag{12}$$

where κ is the thermal conductance, θ_0 is the ambient temperature. The dissipated averaged power over one period of an oscillation $\overline{P(t)}$ is

$$\overline{P(t)} = \gamma(\theta)\langle \dot{X}_{0'}^2 \rangle = \gamma(\theta)\frac{1}{T}\int_0^T \text{Re}\{X_{0'}(t)\}^2 dt$$
$$= \frac{\gamma(\theta)\omega^2}{2}(\text{Re}\{a_{0'}\}^2 + \text{Im}\{a_{0'}\}^2). \tag{13}$$

Substitution of the above expression in Eq. (12) allows us to evaluate the steady-state temperature θ_∞ of the system of coupled oscillators, for a given incident wave amplitude $I_{L/R}$ and wave number k. Specifically, θ_∞ is evaluated numerically as the root of the nonlinear Eq. (12) after imposing the steady-state condition $\frac{d\theta(t)}{dt} = 0$ [39]. The next step is to substitute θ_∞ in the expression (11) in order to evaluate the corresponding steady-state value γ_∞. The latter is then used in Eqs. (7) and (9) for the evaluation of the steady-state values of $\mathcal{T}_L$, $\mathcal{T}_R$.

Some representative cases of the steady-state values of left and right transmittances, transmission phases $\phi_{L/R}$, and
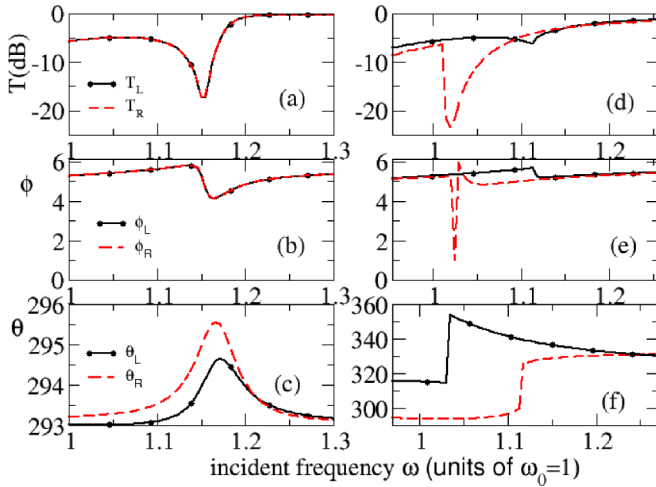
FIG. 5. Transport properties of the toy model of Eqs. (3a)–(3c). Left column: (a) transmittance $T_{L/R}$, (b) transmission phase $\phi_{L/R}$, and (c) temperature $\theta_{L/R}$ spectra for a CW wave with field amplitude 0.5. Left (solid black lines) and right (dashed red lines) incident signal is indicated with the subindex L/R. (d) $T_{L/R}$, (e) $\phi_{L/R}$, and (f) $\theta_{L/R}$ for an incident wave with field amplitude 3. The transport behavior is in one-to-one relation with the results from the photonic circuit (see Figs. 2 and 3).

temperatures $\theta_{L/R}$ of the oscillator $0'$ vs frequency for small $I_{L/R} = 0.5$ (left column) and intermediate $I_{L/R} = 3$ (middle column) values of the incident wave are shown in Fig. 5. The other parameters used are $\omega_0 = 1$, $\omega_c = \omega_l = 0.7$, $\gamma_{\min} = \kappa = 0.02$, $\gamma_{\max} = 10$, $\theta_c = 342$, $\theta_0 = 293$, $\Delta = 5$. We focus our analysis on the antisymmetric resonance (the system shows another resonance for lower frequencies, associated with a symmetric mode of the coupled dimer oscillator). A direct comparison with the transport results of the photonic circuit (see Figs. 2 and 3) indicates that our system shows the same qualitative behavior. Specifically, there are two transport regimes associated with the incident field intensity: for low intensities the system shows bidirectional Fano resonances. In this regime, the asymmetry in the left and right transmittances is (if at all!) minimal. In contrast, when the intensity of the incident wave takes intermediate values, the asymmetry becomes maximum. A simple inspection of Fig. 5(c) indicates that the origin of the asymmetric transport is the directional (i.e., from the left) heating of the oscillator $n = 0'$ and the consequent increase of its friction coefficient γ which leads to suppression of the Fano resonance [see Figs. 5(a) and 5(b)]. One way to understand this asymmetric heating is by realizing that the transmitted energy towards the oscillator $n = 0'$ involves only one scattering event at the junction $n = 0$, while an incident wave from the right requires at least two scattering events in order to reach the lossy oscillator.

Although the toy model that we have developed here is simple, it retains the basic physics principles that are responsible for the observed asymmetry in the transport properties of the photonics circuit of the previous section. It is analytically tractable and can potentially be explored further in order to better understand the transport near the phase-change transition point. In this case, the phase stability of the high-temperature regime and the hysteresis effects due to the

heating and cooling cycles have to be carefully analyzed in order to obtain a better picture of the transport properties of our setup. The investigation along these lines will cast more light on the physics of photonic structures based on PCM and will be the subject of future work.

IV. CONCLUSIONS

We have studied the transport properties of an asymmetric photonic circuit made of two microresonators side coupled to a bus waveguide. One of them consists of a phase-change material (PCM) and undergoes a phase transition from an insulating to a metallic phase due to self-induced heating by the incident radiation. For low incident irradiances, the photonic circuit supports Fano resonances, associated with interference between a high-Q resonant mode of the photonic circuit and a scattering state inside the continuum of states supported by the bus waveguide. In this case, Fano resonance is bidirectional and the transmittance asymmetry between left and right incident waves is minimal (if at all). For higher irradiances of the incident radiation, the Fano resonance is unidirectional. The phenomenon is associated with the degradation of the Q factor of the resonant mode when the light enters the structure from the side of the PCM resonator. We show that in this case the transmittance asymmetry is maximal and can reach values as high as 45 dBs. Our numerical results for the optical photonic circuit are quantitatively captured by a simple mechanical model consisting of two coupled oscillators where one of them has a temperature-dependent friction coefficient.

The photonic circuit that we have investigated operates at the long-wave infrared range (LWIR). One reason is that our simple setting based on an asymmetric pair of coupled microresonators (of which one is loaded with VO_2) will not work at telecom wavelengths. Indeed, the change in the imaginary part of the VO_2 refractive index, associated with the insulator-to-metal phase transition, is strongly dependent of the wavelength. At telecom wavelengths, this change is not large enough to produce the desired effect. It does not mean, though, that the use of PCM for our purposes is absolutely restricted to longer wavelengths. What it really means is that, first, we would need a more sophisticated photonic structure and, second, the performance will be less impressive especially when it comes to the bandwidth and the activation time. Currently, we are working on the experimental realization of our original idea for LWIR. At the same time, we are exploiting more complex designs, based on Fano microresonators coupled to an optical waveguide, that will demonstrate similar level of switching efficiency at shorter wavelengths.

[1] B. E. A. Saleh and M. C. Teich, *Fundamentals of Photonics* (Wiley, New York, 1991).

[2] J. D. Joannopoulos, S. G. Johnson, J. N. Winn, and R. D. Meade, *Photonic Crystals: Modeling the Flow of Light* (Princeton University Press, Princeton, NJ, 2008).

[3] P. A. Deymier, *Acoustic Metamaterials and Phononic Crystals* (Springer, Berlin, 2013).

[4] A. A. Maznev, A. G. Every, and O. B. Wright, Reciprocity in reflection and transmission: What is a phonon diode? Wave Motion **50**, 776 (2013).

[5] R. Fleury, D. Sounas, M. R. Haberman, and A. Alu, Nonreciprocal acoustics, Acoustics Today **11**, 14 (2015).

[6] S. Datta, *Quantum Transport: Atom to Transistor* (Cambridge University Press, Cambridge, 2005).

[7] A. K. Zvezdin and V. A. Kotov, *Modern Magnetooptics and Magnetooptical Materials* (Taylor & Francis, London, 1997).

[8] X. Y. Sun *et al.*, Single-step deposition of cerium-substituted yttrium iron garnet for monolithic on-chip optical isolation, ACS Photonics **2**, 856 (2015).

[9] K. Shui *et al.*, Design of a compact waveguide optical isolator based on multimode interferometers using magneto-optical oxide thin films grown on silicon-on-insulator substrates, Opt. Express **24**, 12856 (2016).

[10] Z. Yu and S. Fan, Complete optical isolation created by indirect interband photonic transition, Nat. Photonics **3**, 91 (2009).

[11] K. Fang, Z. Yu, and S. Fan, Photonic Aharonov-Bohm Effect Based on Dynamic Modulation, Phys. Rev. Lett. **108**, 153901 (2012).

[12] H. Lira, Z. Yu, S. Fan, and M. Lipson, Electrically Driven Nonreciprocity Induced by Interband Photonic Transition on a Silicon Chip, Phys. Rev. Lett **109**, 033901 (2012).

[13] K. Fang, Z. Yu, and S. Fan, Realizing effective magnetic field for photons by controlling the phase of dynamic modulation, Nat. Photonics **6**, 782 (2012).

[14] L. D. Tzuang, K. Fang, P. Nussenzveig, S. Fan, and M. Lipson, Non-reciprocal phase shift induced by an effective magnetic flux for light, Nat. Photonics **8**, 701 (2014).

[15] N. A. Estep, D. L. Sounas, J. Soric, and A. Alu, Magnetic-free non-reciprocity and isolation based on parametrically modulated coupled-resonator loops, Nat. Phys. **10**, 923 (2014).

[16] A. B. Khanikaev and A. Alu, One-way photons in silicon, Nat. Photonics **8**, 680 (2014).

[17] D. L. Sounas, C. Caloz, and A. Alu, Giant non-reciprocity at the subwavelength scale using angular momentum-biased metamaterials, Nat. Commun. **4**, 2407 (2013).

[18] H. Ramezani, T. Kottos, R. El-Ganainy, and D. N. Christodoulides, Unidirectional nonlinear $\mathcal{PT}$-symmetric optical structures, Phys. Rev. A **82**, 043803 (2010).

[19] S. Lepri and G. Casati, Asymmetric Wave Propagation in Nonlinear Systems, Phys. Rev. Lett. **106**, 164101 (2011).

[20] N. Bender, S. Factor, J. D. Bodyfelt, H. Ramezani, D. N. Christodoulides, F. M. Ellis, and T. Kottos, Observation of Asymmetric Transport in Structures with Active Nonlinearities, Phys. Rev. Lett. **110**, 234101 (2013).

[21] F. Nazari, N. Bender, H. Ramezani, M. K. Moravvej-Farshi, D. N. Christodoulides, and T. Kottos, Optical isolation via $\mathcal{PT}$-symmetric nonlinear Fano resonances, Opt. Express **22**, 9574 (2014).

[22] A. B. Khanikaev and A. Alu, Nonlinear dynamic reciprocity, Nat. Photonics **9**, 359 (2015).

[23] D. L. Sounas, J. Soric, and A. Alu, Broadband passive isolators based on coupled nonlinear resonances, Nat. Elec. **1**, 113 (2018).

[24] C. Wan, E. H. Horak, J. King, J. Salman, Z. Zhang, Y. Zhou, P. Roney, B. Gundlach, S. Ramanathan, R. H. Goldsmith, and M. A. Kats, Limiting optical diodes enabled by the phase transition of vanadium dioxide, ACS Photonics **5**, 2688 (2018)

[25] N. Antonellis, R. Thomas, M. A. Kats, I. Vitebskiy, T. Kottos, Asymmetric transmission in photonic structures with phase-change components, arXiv:1806.07514.

[26] D. N. Basov *et al.*, Mott transition in VO_2 revealed by infrared spectroscopy and nano-imaging, Science **318**, 1750 (2007).

[27] Y. S. Joe, A. M. Satanin, and C. S. Kim, Classical analogy of Fano resonances, Phys. Scr. **74**, 259 (2006).

[28] A. E. Miroshnichenko, S. Flach, and Y. S. Kivshar, Fano resonances in nanoscale structures, Rev. Mod. Phys. **82**, 2257 (2010).

[29] D. Fausti, R. I. Tobey, N. Dean, S. Kaiser, A. Dienst, M. C. Hoffmann, S. Pyon, T. Takayama, H. Takagi, and A. Cavalleri, Light-induced superconductivity in a stripe-ordered cuprate, Science **331**, 189 (2011).

[30] F. J. Morin, Oxides Which Show a Metal-to-Insulator Transition at the Neel Temperature, Phys. Rev. Lett. **3**, 34 (1959).

[31] D. N. Basov, R. D. Averitt, D. V. Marel, M. Dressel, and K. Haule, Electrodynamics of correlated electron materials, Rev. Mod. Phys. **83**, 471 (2011).

[32] T. Peterseim, T. Ivek, D. Schweitzer, and M. Dressel, Electrically induced phase transition in α-$(BEDT-TTF)_2I_3$: Indication for Dirac-like hot charge carriers, Phys. Rev. B. **93**, 245133 (2016).

[33] M. Xua, Y. Q. Chenga, L. Wang, H. W. Shenge, Y. Meng, W. G. Yang, X. D. Hang, and E. Maa, Pressure tunes electrical resistivity by four orders of magnitude in amorphous $Ge_2Sb_2Te_5$ phase-change memory alloy, Proc. Natl. Acad. Sci. USA **109**, E1055 (2011).

[34] J. Locquet, J. Perret, and J. Fompeyrine, Doubling the critical temperature of $La_{1.9}Sr_{0.1}CuO_4$ using epitaxial strain, Nature (London) **394**, 453 (1998).

[35] M. A. Kats, R. Blanchard, P. Genevet, Z. Yang, M. M. Qazilbash, D. N. Basov, S. Ramanathan, and F. Capasso, Thermal tuning of mid-infrared plasmonic antenna arrays using a phase change material, Opt. Lett. **38**, 368 (2013).

[36] COMSOL MULTIPHYSICS v. 5.2, www.comsol.com COMSOL AB, Stockholm, Sweden.

[37] R. Thomas, I. Vitebskiy, and T. Kottos, Resonant cavities with phase-changing materials, Opt. Lett. **42**, 4784 (2017).

[38] R. Thomas, F. M. Ellis, I. Vitebskiy, and T. Kottos, Self-regulated transport in photonic crystals with phase-changing defects, Phys. Rev. A **97**, 013804 (2018).

[39] For some parameter ranges, the heat rate equation has multiple roots, thus exhibiting multistabilities. In these cases, we considered as the steady-state solution the maximum temperature obtained that corresponded to a root and for which the second time derivative of the temperature is negative.